EMPLOYING IMAGEJ SOFTWARE AS A MEASUREMENT TOOL FOR OPTICS EXPERIMENTS IN THE DIDACTIC LABORATORY

ADRIANA RADU[1,2,#], M. V. POPESCU[3,#], C. BERLIC[1,*,#], CRISTINA MIRON[1.*,#], V. BARNA[1,#]

[1] University of Bucharest, Faculty of Physics, 405 Atomistilor Street, 077125, Magurele, Romania
[2] National College "Mihai-Viteazul", 8 Independentei Avenue, Ploiesti, Romania
[3] National College "Ion Luca Caragiale", 98 Gheorghe Doja Street, Ploiesti, Romania

*Corresponding authors: cberlic@gmail.com, cmiron_2001@yahoo.com

[#] All authors equally contributed to this work as first author.

Received

Abstract. In this paper, we employed ImageJ as an image processing software for the analysis of the data obtained from experiments in the optics physics laboratory. We used the software to investigate the interference and diffraction patterns obtained from Newton's rings, Fresnel biprism, and the diffraction patterns acquired by diffraction gratings. ImageJ is a free software that is extensively used in scientific research for measurement and inquiry. The program is easy to use and merely demands computational hardware resources that can be found on usual computers. It is also easy to understand by most of the students while being very efficient and accurate. This tool is extremely useful and precise, helping the students to focus on understanding the concepts. It can be also adapted to many laboratories assisting to improve their educational aptitudes.

Key words: image processing software, ImageJ, optics experiment, physics education.

1. INTRODUCTION

Nowadays, the use of the computer and digital methods of obtaining and processing data from experiments are widely used in teaching physics [1, 2]. Classical experiments adapted to an experimental framework containing computer technologies are also able to stimulate the development of students' creative thinking [3], to generate new ideas, concepts and technologies. For example, the Tracker software was used as video analysis tool [4 - 9], Audacity was used as audio analysis tool [10 - 12], or special developed software for simulation and modeling [13 - 16] was used.

In this paper, we present a method of processing interference patterns obtained from optics classes experiments, by means of the ImageJ software.

ImageJ is open source image processing and analysis software, developed by Wayne Rasband of the National Institute of Health (NIH), USA [17]. The ImageJ software has the advantage that it is free and independent of any hardware vendor and operating system [18]. ImageJ, originally developed for life sciences, is a useful tool for any field that benefits from visualization, image processing, and analysis such as earth sciences, astronomy, fluid dynamics or signal processing. [19]. ImageJ is an ideal platform for education and training using digital image processing [20]. It became a useful tool in many research or educational laboratories around the world because it is very complex, free and easy to use. Furthermore, it can be used by non-experts for image processing, since it is user-friendly, with extensive tutorial materials available [21].

The ImageJ software can display, edit, analyze, process, save and print images in various formats. It can interpret common image formats and perform basic operations such as image sharpening, grayscale conversion, contrast enhancement and cropping. So, it becomes a valuable tool in performing various types of measurements involving images [22]. With ImageJ, various statistical calculations can be done for certain areas of an image selected by the user or for the entire image. It also measures distances, angles and areas [23].

2. EXPERIMENTS AND METHODS

2.1. Newton's rings

"Newton's rings" appear as the result of the interference of the monochrome light in the thin intermediate gap between a flat-convex lens and a flat glass plate [24, 25]: beam 1, reflected from the bottom of the convex lens, interferes with beam 2, reflected from the top of the glass plate as shown. Figure 1 schematically presents the construction of the Newton rings.

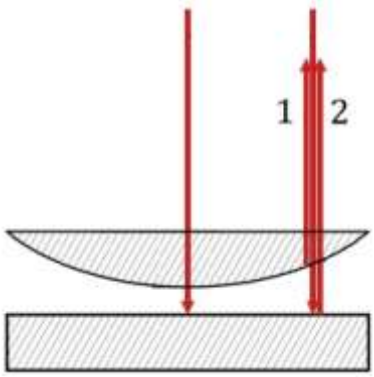

Fig. 1 – Construction of the Newton rings. The full color version may be accessed at http://www.rrp.infim.ro/rrp/.

Figure 2 is the image of the experimental setup we used in the didactic framework of the laboratory.

The experimental set-up consists of a power source (1) which drives a mercury vapor high-pressure lamp fitted with a double condenser (with focal length 60 mm) (2), monochrome filter holder (3), "Newton's rings" optical system with graduated lattice scale (4), converging lens (5) and the translucent observation screen (6).

A green monochrome filter was used, while the image with the dark and light rings is obtained on the screen. With the help of a digital camera placed behind the translucent screen, images of the rings are obtained.

Fig. 2 – Experimental setup for the observation of Newton rings. The full color version may be accessed at http://www.rrp.infim.ro/rrp/.

In this paper we employed the ImageJ software in order to find the radius of the dark rings obtained on the translucent screen (see Figure 3).

Since the image was opened in ImageJ, in order to have access to its image-processing methods, the conversion of the image to grayscale was performed using the commands: Image → Type→ 16 bit, as shown in Figure 3.

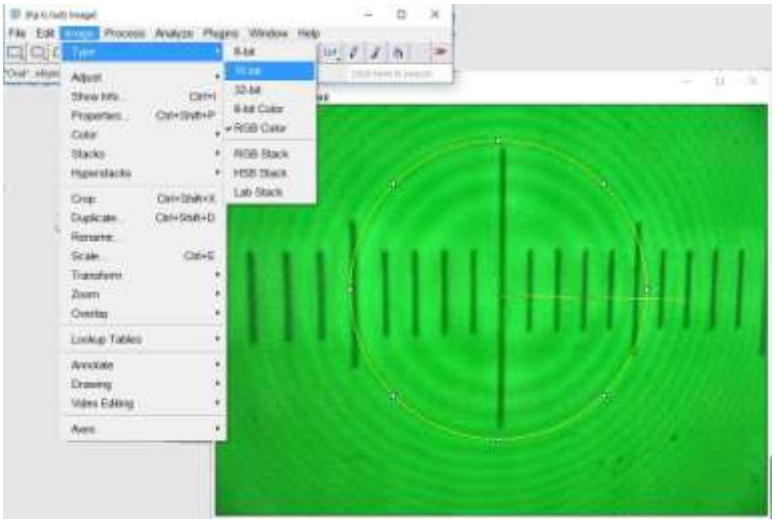

Fig. 3 – Steps used for the conversion to a gray scale image. The full color version may be accessed at http://www.rrp.infim.ro/rrp/.

In order to choose the parameters we need to measure, the commands: Analyze → Set Measurements were used. For this experiment, the measured parameter was the radius of the dark ring. The first step is the scale calibration. Using the menu item "Straight Line Selection Tool" from the menu bar, one can measure on an image a known distance and then use the commands: Analyze → Set Scale, as shown in Figures 4 and 5.

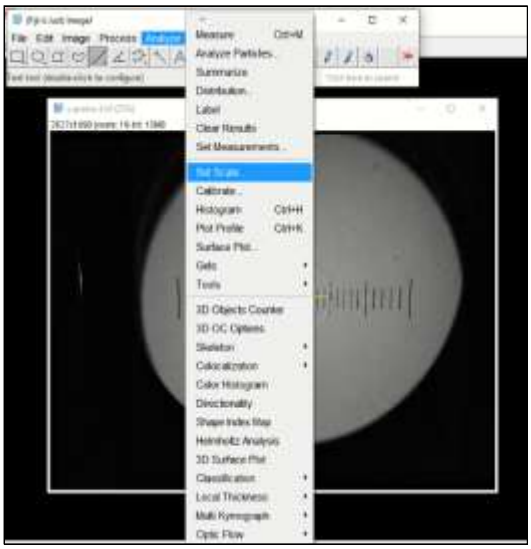

Fig. 4 – Steps used to calibrate the scale. The full color version may be accessed at http://www.rrp.infim.ro/rrp/.

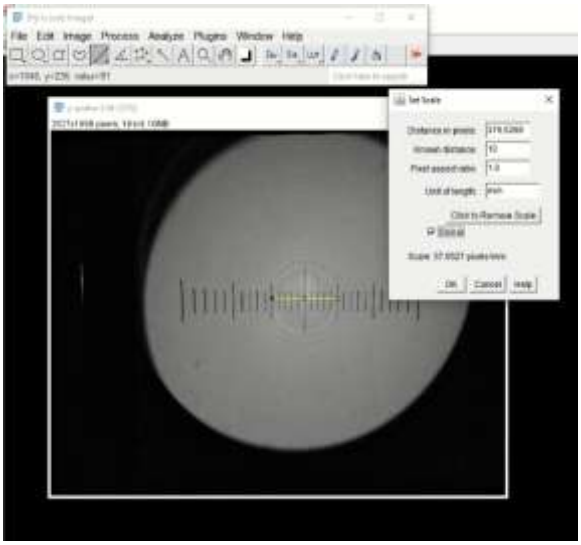

Fig. 5 – Setting the scale. The full color version may be accessed at http://www.rrp.infim.ro/rrp/.

Subsequently, by using the menu item "Straight Line Selection Tool", the radius of a dark ring was drawn. We then use the Analyze → Measure options. The measurement results were saved in a format specific to spreadsheet applications. The values of the radius of the dark rings (interference minimum) are presented in Table 1.

Table 1

Measured values of the radius of the dark rings obtained using the green filter

Order (n)	r_n [mm]
1	3.129
2	3.865
3	4.568
4	5.268
5	6.029
6	6.399
7	7.037

The graph showing the dependence of the square of the radius of the dark ring of its order n, $r_n^2 = f(n)$, is presented in Figure 6.

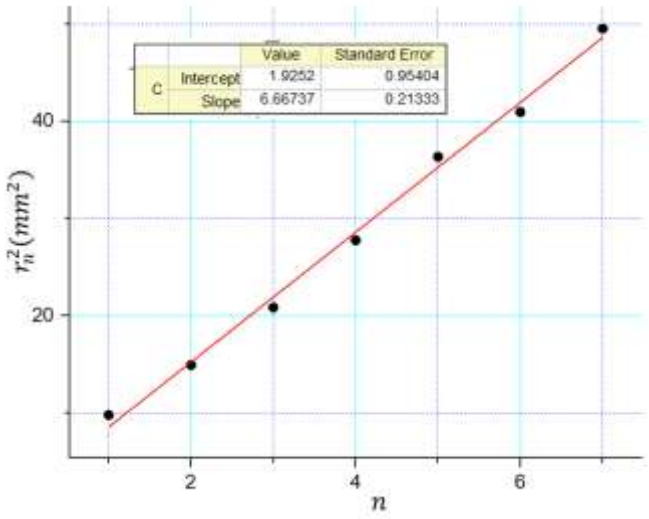

Fig. 6 –Dependence of the square of the radius of the dark ring of its order n. The full color version may be accessed at http://www.rrp.infim.ro/rrp/.

From Figure 6 one can deduce that the slope of the interpolation line is $tg\ \alpha = 6.67\ mm^2$.

The wavelength calculated from the equation $\lambda = \frac{tg\ \alpha}{R}$, where $R = 12.141\ m$ is the radius of curvature of the lens, is $\lambda_{g,1} = 549\ nm$.

The wavelength of the light transmitted by the green filter used in the

experiment is $\lambda_g = 545\,nm$, following that the accuracy offered by the ImageJ program is quite high.

A similar result can be obtained using another measurement method offered by the ImageJ software. We can determine the area of the rings and graphically represent the values of the measured area according to the order n of the ring. With the option Set Measurements, we chose Area. We then calibrated the scale, according to the steps previously described. With the help of the "Oval Selection Tool", we selected the ring, after which we used the option Analyze → Measure, as shown in Figure 7.

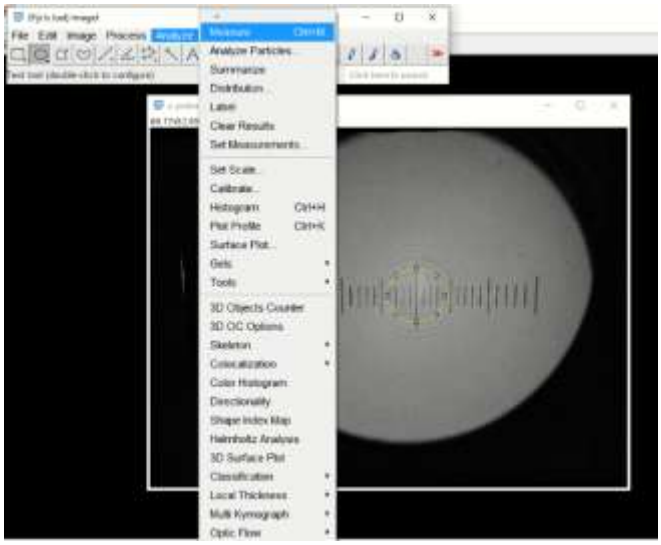

Fig. 7 – Making the selection to measure the area of the ring with ImageJ. The full color version may be accessed at http://www.rrp.infim.ro/rrp/.

We determined the area of each dark ring. The results calculated by ImageJ are printed in a table, as shown in Figure 8.

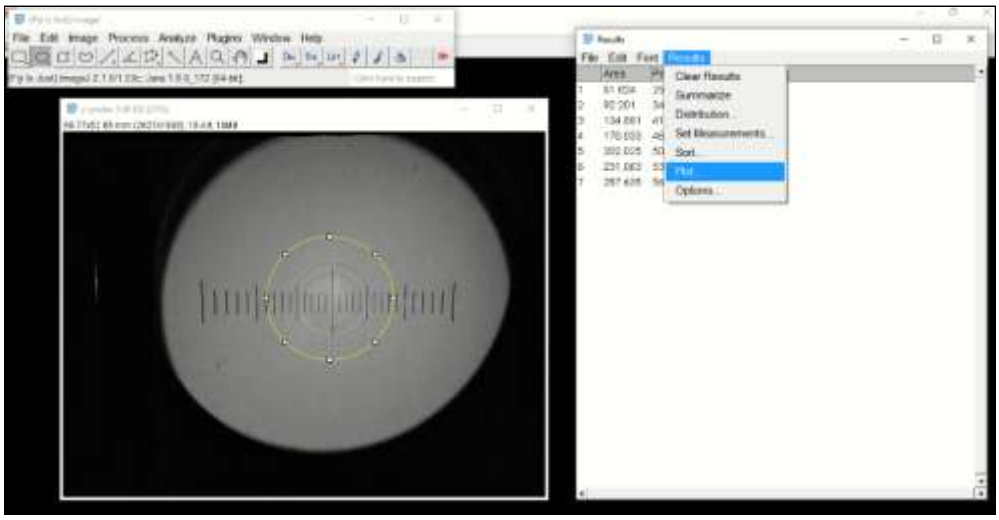

Fig. 8 – Displaying the values of the areas of the dark rings and selecting the option to graphically represent the measured area by ring order n. The full color version may be accessed at http://www.rrp.infim.ro/rrp/.

By activating the option Results → Plot, the graph of the area as a function of the order n of the dark ring appears as in Figure 9.

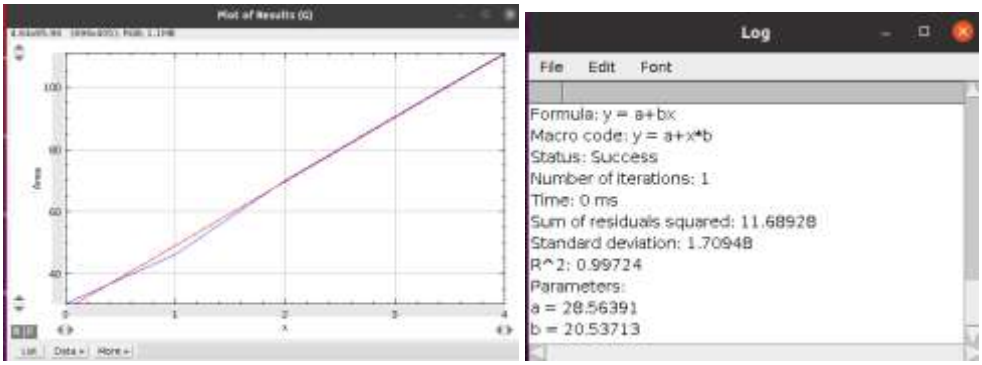

Fig. 9 – The graphical representation of the area measured according to the order of the ring. The full color version may be accessed at http://www.rrp.infim.ro/rrp/.

The slope of the interpolation line is $tg\ \alpha = 20.537\ mm^2$. The wavelength of the radiation was determined from the relation $\lambda = \dfrac{tg\ \alpha}{\pi R}$, where $R = 12.141\,m$. The value obtained for the wavelength is $\lambda_{g,2} = 538\ nm$.

The radius of the rings was also determined by direct viewing on the observation screen. These obtained results are presented in Table 2.

Table 2

Radius of the dark green rings obtained by direct visualization

Order (n)	r_n [mm]
1	3.40
2	4.69
3	5.38
4	5.91
5	6.32
6	6.92
7	7.14

Furthermore, the graph of the square of the radius of the dark green rings as function of the order of the ring is shown in Figure 10.

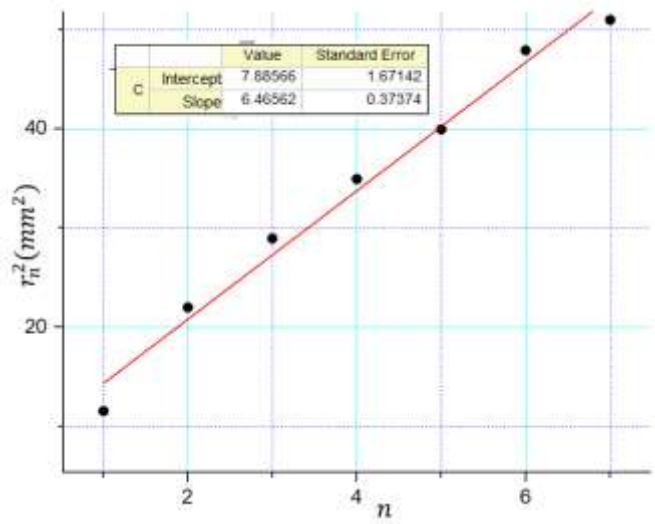

Fig. 10 – Graph of the square of the radius of the dark green rings as function of the order of the ring. The full color version may be accessed at http://www.rrp.infim.ro/rrp/.

From the graph in Figure 10, the slope of the interpolation line is $tg\ \alpha = 6.46\ mm^2$. The wavelength obtained from the equation $\lambda = \frac{tg\ \alpha}{R}$, where $R = 12.141\ m$ is $\lambda_{g,3} = 532\ nm$, whereas the wavelength of the light transmitted

by the green filter used is $\lambda_g = 545\ nm$. We conclude that the wavelength of the radiation determined with ImageJ, $\lambda_{g,1} = 549\ nm$, respectively $\lambda_{g,2} = 538\ nm$ are closer to the actual one, rather than the one determined by direct measurements ($\lambda_{g,3} = 532\ nm$).

2.2. The Fresnel Biprism

The Fresnel biprism is made up of two thin prisms joint to form an isosceles triangle, Fig. 11. The refractive angle of the prism is very small.

A wavefront from a light source falls on both prisms, the upper portion of the wavefront is refracted right while the bottom fraction is refracted left [26]. The two beams behave as two close coherent virtual sources approximately formed in the plane of the initial source. The waves from the virtual sources overlap providing interference.

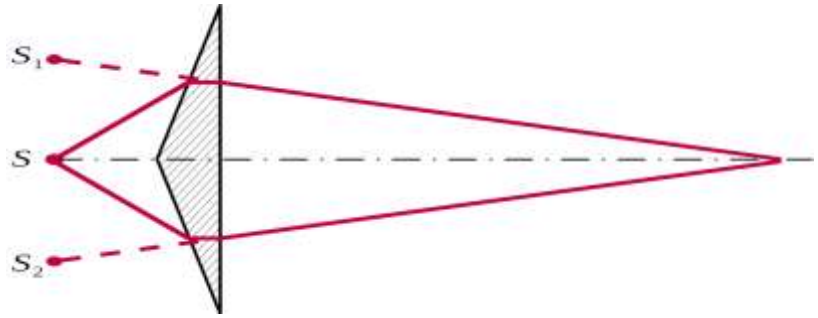

Fig. 11 – Formation of virtual images of the source through the Fresnel biprism [23]. The full color version may be accessed at http://www.rrp.infim.ro/rrp/.

We used as a monochromatic light source a HeNe laser placed in front of the biprism as a wave source, Figure 12. In order for the beam to reach the biprism mount, it must be expanded using a converging lens. The source S is positioned in the focus of this lens.

Fig. 12 – The experimental set-up for light interference with the Fresnel biprism. The full color version may be accessed at http://www.rrp.infim.ro/rrp/.

The components mounted on the optical bench from Figure 12 are: (1) monochrome light source – a $1\,mW$ laser with HeNe; (2) converging lens with focal length $f_1 = 20\,mm$; (3) mount with the Fresnel biprism; (4) convergent lens with focal length $f_2 = 300\,mm$ used to form the image of the two virtual sources; (5) translucent screen on which we observe the image of the two virtual sources and the interference bands.

In the overlapping region of the two beams, equidistant bands are obtained on an observation screen. In this experiment, the interfringe and the distance between the projected images on the screen of the two sources are determined. The projection of the images of the virtual sources on the screen is done with the help of a converging lens. The wavelength of the radiation used is obtained from the relation $\lambda = \frac{ia}{L}$, where i is the interfringe, a is the distance between the images between the two virtual sources obtained on the screen and L is the distance between the plane of the source and the screen.

In the present work, we used two different radiations: red and green. Figure 13 shows the image of the virtual sources for the red radiation.

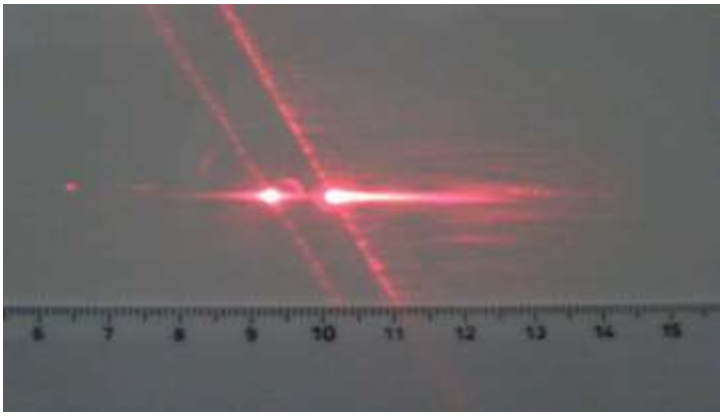

Fig. 13 – The image of the virtual sources in the red light. The full color version may be accessed at http://www.rrp.infim.ro/rrp/.

To obtain the distance between the images of the virtual sources and the value of the interband we again employed the ImageJ program. After setting the scale, with the help of "Straight Line Selection Tool" from the menu bar, we traced a straight line corresponding to the distance between the two images, then we used the option: Analyse → Measure.

Using the same procedure, we determined the interfringe, by measuring the distance between ten consecutive bands. The obtained results are shown in the table Plot Values from Figure 14.

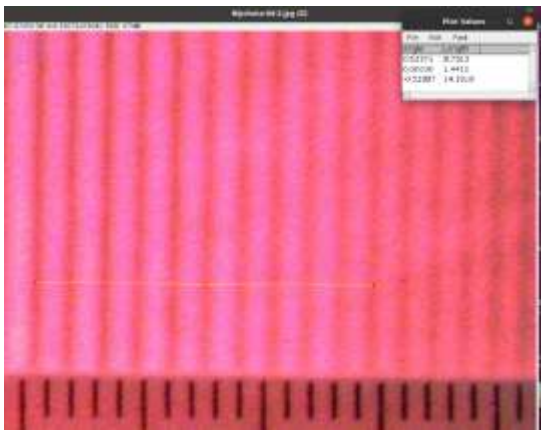

Fig. 14 – The interference bands in red light and the Plot Values. The full color version may be accessed at http://www.rrp.infim.ro/rrp/.

Concluding, the distance between the images of the virtual sources is $A = 8.731\,mm$, the interband is $i = 1.44\,mm$ and the distance between ten

consecutive bands is equal to $14.191\,mm$, the interband in this case having the value $i = 1.41\,mm$.

In Figure 15, it is represented the graph for the distribution of the illumination level for the bands as function of distance.

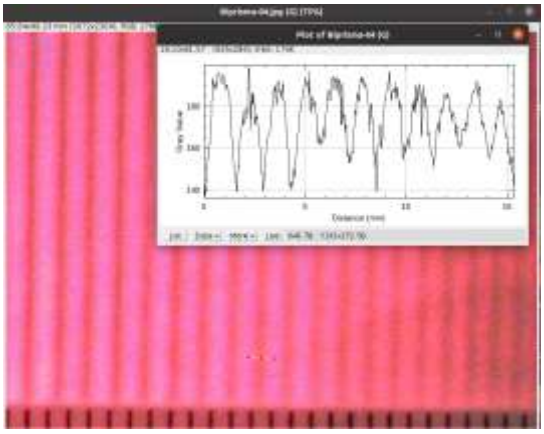

Fig. 15 – The distribution of the illumination level for the bands in the red light. The full color version may be accessed at http://www.rrp.infim.ro/rrp/.

Using the same procedure, we made the determinations for the green radiation.

In Figure 16 it is represented the image of the virtual sources for the green radiation, whereas in Figure 17 are shown the bands obtained on the screen.

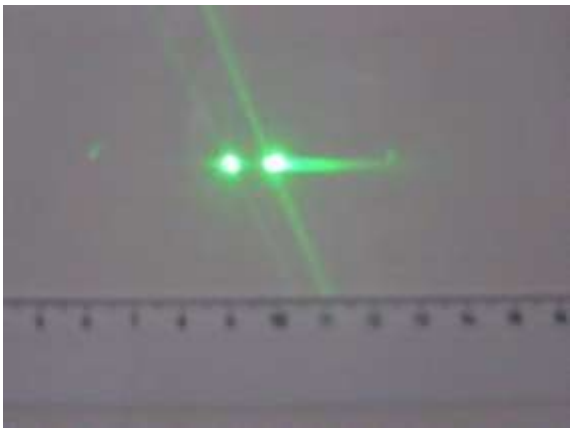

Fig. 16 – The image of the virtual sources in green light. The full color version may be accessed at http://www.rrp.infim.ro/rrp/.

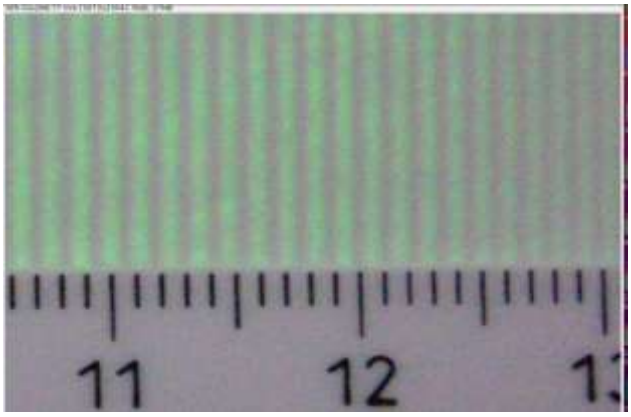

Fig. 17 – The interference bands in green light. The full color version may be accessed at http://www.rrp.infim.ro/rrp/.

The distance between the images of the virtual sources is $A = 9.02\ mm$, the interfringe is $i = 1.07\ mm$ and the distance between ten consecutive bands is equal to $11.053\ mm$, therefore the interfringe in this case is $i = 1.10\ mm$.

The wavelength was calculated from the formula $\lambda = \frac{ia}{L}$. The data obtained are presented in Table 3.

Table 3

Result obtained after processing the images

Type of radiation	L_0 [cm]	L_1 [cm]	L_2 [cm]	L [cm]	A [mm]	a [mm]	i [mm]	λ [nm]
Red	38.2	36.2	245	281.2	8.731	1.29	1.44	660
Green	38.2	36.2	245	281.2	9.02	1.33	1.10	521

The wavelength of the red radiation is $632\ nm$ and for the green one is $533\ nm$.

2.3. Diffraction grating

By means of the ImageJ program we studied the pattern obtained using the diffraction grating. The experimental set-up is presented in Figure 18 and consists of a laser pointer (1), a diffraction grating (2) and a translucent screen (3).

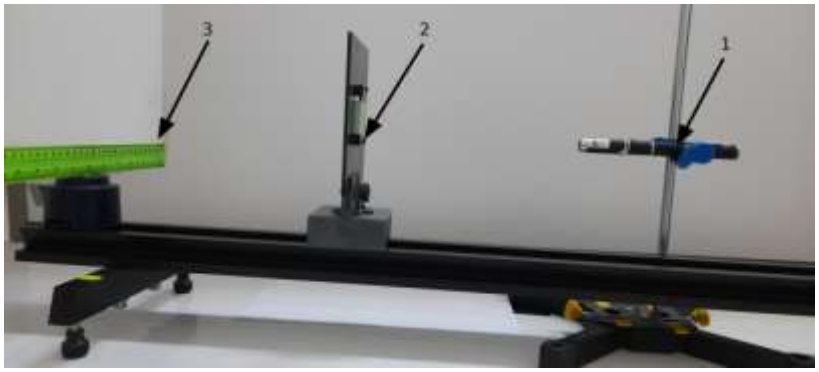

Fig. 18 – Experimental set-up for the diffraction grating. The full color version may be accessed at http://www.rrp.infim.ro/rrp/.

To obtain the diffraction image, we used a laser pointer with red radiation, a diffraction grating and a screen on which the diffraction band was observed.

The diffraction grating with $15000\ features/inch$ has the constant $l = 1.69 \cdot 10^{-6} m$.

The wavelength of the radiation used is determined with the formula: $\lambda = \frac{ly}{nd}$, where, l is diffraction grating constant, y is the position of a maximum of order n, and d is the distance between the plane of the diffraction grating and the screen on which the diffraction pattern is obtained.

The image of the diffraction pattern obtained with the diffraction grating in red light is presented in Figure 19.

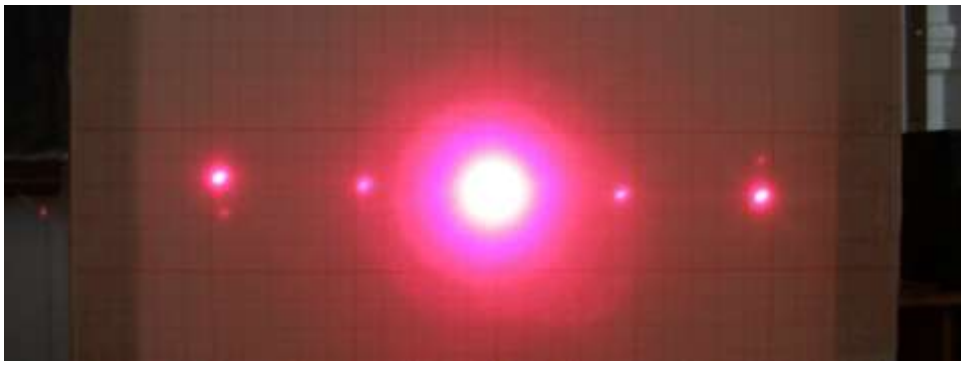

Fig. 19 – The diffraction pattern obtained by grating in red light . The full color version may be accessed at http://www.rrp.infim.ro/rrp/.

Table 4

Data obtained from light diffraction using red radiation

No.	l [m]	d [m]	n	y_i [m]	λr [nm]	$\lambda_{r,ave}$ [nm]
1.	$1.69 \cdot 10^{-6}$	$12 \cdot 10^{-2}$	1	$45.550 \cdot 10^{-3}$	641	654
2.			2	$94.803 \cdot 10^{-3}$	667	

In the ImageJ software we obtained the graphic representation of the illumination levels from the diffraction pattern according to the position y_i on the screen for the employed grating.

For the diffraction pattern measurements the following routine steps are followed: using the "Straight Line Selection Tool" from the menu bar, we traced the distance between the two maximums of the second order, then we used the option: Analyze → Plot Profile, as shown in Figure 20.

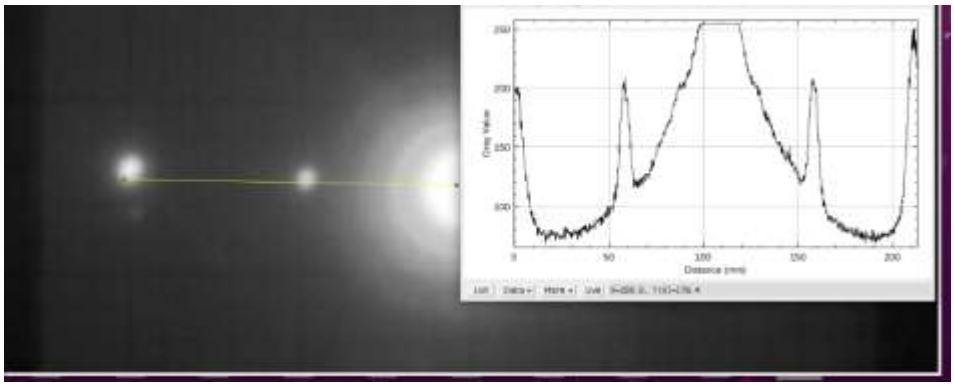

Fig. 20 – Distribution of the values of the illumination intensity on the diffraction pattern according to the y_i position. The full color version may be accessed at http://www.rrp.infim.ro/rrp/.

The red laser diode pointer light source the has an emission at $\lambda_r = 650\,nm$, while we experimentally obtained $\lambda_{r,ave} = 654\,nm$. The results are in very good agreement.

We then repeated the measurements, this time by using a green laser pointer, with $\lambda_g = 533\,nm$. In Figure 21 it is shown the diffraction pattern and in Table 5 we have the data processed using ImageJ.

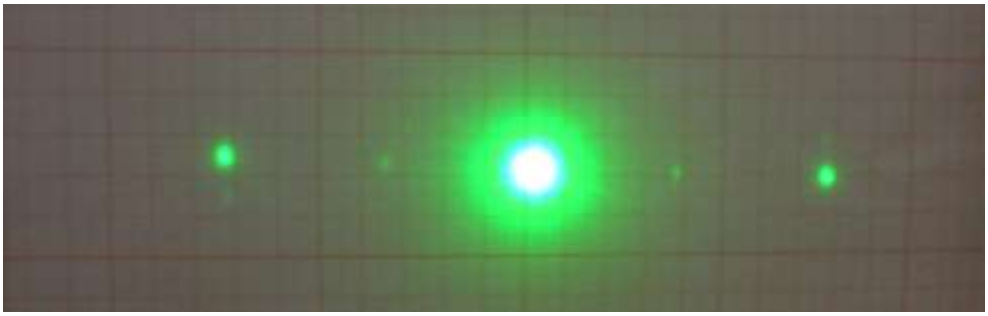

Fig. 21 – Diffraction pattern obtained using the diffraction grating in green light. The full color version may be accessed at http://www.rrp.infim.ro/rrp/.

Table 5

Data processing regarding light diffraction using green light

No.	l [m]	d [m]	n	y_i [m]	λ_g [nm]	$\lambda_{g,ave}$ [nm]
1.	$1.69 \cdot 10^{-6}$	$12 \cdot 10^{-2}$	1	$37.715 \cdot 10^{-3}$	531	533
2			2	$76.051 \cdot 10^{-3}$	535	

One can notice that the average value obtained for green radiation by using ImageJ is identical to that of the laser-pointer radiation.

The graphical representation of the distribution of the values of the illumination intensity on the diffraction pattern in green light according to the y_i position on the screen for the employed grating is presented in Figure 22.

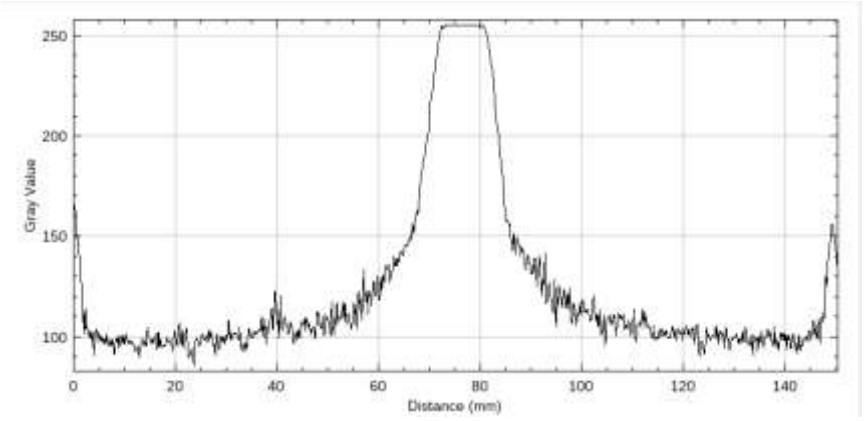

Fig. 22 – Graph of illumination according to the distance for diffraction in green light. The full color version may be accessed at http://www.rrp.infim.ro/rrp/.

3. CONCLUSIONS

In the present paper, we used the image processing technique as a measurement tool for optics experiments in the didactic physics laboratory, by means of the ImageJ software.

ImageJ represents a free and open-source useful tool for fields of activity that involve image processing and analysis. At the same time, the application allows for obtaining graphic representations associated with the analyzed images, such as the representation of the distribution of the levels of illumination intensity on the surface of an image both in color and in shades of gray. The interface of the application is user-friendly, with many extension possibilities and it is overall very easy to handle. ImageJ is very useful in optics lessons for measuring interfringes, radii and angles. It is easy to use by students, the data processing being visibly faster than in the case of classical experiments, while the obtained data are very accurate. The students have also the possibility to carry out a complex activity, starting from acquiring the images of the interference and diffraction patterns with digital cameras or with high-performance smartphones, then continuing with the processing of these images with the ImageJ software. They can afterwards analyze the data by building various graphs, fitting the data and handling the image processing part. The method described herein for image processing can be extensively employed to further improve understanding of other physics concepts and use the experiments as a way to achieve better learning results.

REFERENCES

1. S. Panarin, J. Mueller, S. Prabhakar, R. Fickler, Robert, Am. J. Phys. **89**(2), 210-219 (2021).
2. M. Riaz, A. Bashir, M. Bashir, Eur. J. Phys. **39**(6), 065501 (2018).
3. A. Malureanu, G. Panisoara, I. Lazar, Sustainability, **13**(12), 6633 (2021).
4. L. N. Goncalves, J. Fernandes, A. Ferraz, A. G. Silva, P. J. Sebastiao, Am. J. Phys. **88**(11), 962-975 (2020).
5. F. S. Chiriacescu, B. Chiriacescu, C. Miron, C. Berlic, V. Barna, V., Rom. Rep. Phys. **72**(3), 904 (2020).
6. M. Monteiro, F. Tornaria, A. C. Marti, Eur. J. Phys. **41**(3), 035005 (2020).
7. B. Chiriacescu, F. S. Chiriacescu, C. Miron, C. Berlic, V. Barna, Rom. Rep. Phys. **72**(1), 901 (2020).
8. M. Zeuner, K. Schwark, C. Hanisch, M. Ziese, Eur. J. Phys. **40**(6), 065101 (2019).
9. S. Trocaru, C. Berlic, C. Miron, V. Barna, Rom. Rep. Phys. **72**(1), 902 (2020).
10. J. A. Gomez-Tejedor and J. A. Monsoriu, Juan A. Eur. J. Phys. **36**(5), 055036 (2015).
11. F. S. Chiriacescu, B. Chiriacescu, C. Miron, C. Berlic, V. Barna, V., Rom. Rep. Phys. **73**(2), 904 (2021).
12. M. Muradoglu, E. M. W. Ng and T. W. Ng, Eur. J. Phys. **35**(6), (2014).
13. C. Berlic, V. Barna, B. Manolescu, D. Dena, Dig. J. Nanomater. Bios. **8**(4), 1845 - 1852 (2013).
14. N. Riva, F. Grilli, B. Dutoit, Eur. J. Phys. **42**(4), 045802 (2021).
15. C. Berlic and L. M. Constantinescu, Rev. Chim. **55**(11), 910 - 913 (2004).

16. B. Chiriacescu, F. S. Chiriacescu and S. Voinea, Rom. Rep. Phys. **73**(1), 901 (2021).
17. S. N. Baviskar, Am. Biol. Teach. **73(**9), 554 - 556, (2011).
18. A. Bragin, A. Dubanov, A. Rechitskiy, User Interface Design for a Web-based Image Processing and Analysis System, YSIP 27 - 31 (2017).
19. C. T. Rueden, J. Schindelin, M. C. Hiner, B. E. DeZonia, A. E. Walter, E. T. Arena, K. W. Eliceiri, BMC Bioinformatics **18**, 529 (2017).
20. S. J. Said, J. A. E. Noor, Y. Yueniwati, IRJES **3(**7), 24 - 31 (2014).
21. S. van de Linde, J. Phys. D: Appl. Phys. **52**(20), 203002 (2019).
22. J. Alam, A. Shaheen, M. S. Anwar, Eur. J. Phys. **35**(1), 015011 (2014).
23. F. M. Benslimane, Z. Z. Zakaria, S. Shurbaji, M. K. A. Abdelrasool, M. A. H. I. Al-Badr, E. S. K. Al Absi, H. C. Yalcin, Micron **136**, 102876 (2020).
24. F. L. Pedrotti, L. M. Pedrotti, L. S. Pedrotti, *Introduction to Optics*, 3rd Edition, Cambridge University Press, 2018.
25. B. D. Guenther, *Modern Optics Simplified*, Oxford University Press, 2019.
26. F. Chaussard, H. Rigneault, C. Finot, Christophe, Opt. Commun. **397**, 31 - 38 (2017).